Supplementary Information for:

Modular perovskite-$BiVO_4$ artificial leaves towards syngas synthesis on a m^2 scale

Virgil Andrei,[1,2†] Yu-Hsien Chiang,[2†] Motiar Rahaman,[1†] Miguel Anaya,[2,3†] Taeheon Kang,[3]

Edoardo Ruggeri,[2] Samuel D. Stranks,[2,3*] and Erwin Reisner[1*]

[1] *Yusuf Hamied Department of Chemistry, University of Cambridge, Lensfield Road, Cambridge CB2 1EW, United Kingdom.*

[2] *Cavendish Laboratory, University of Cambridge, J J Thomson Avenue, Cambridge CB3 0HE, United Kingdom.*

[3] *Department of Chemical Engineering & Biotechnology, University of Cambridge, Philippa Fawcett Drive, Cambridge CB3 0AS, United Kingdom.*

*Correspondence to: sds65@cam.ac.uk (S.D.S.), reisner@ch.cam.ac.uk (Er.R.).

† These authors contributed equally.

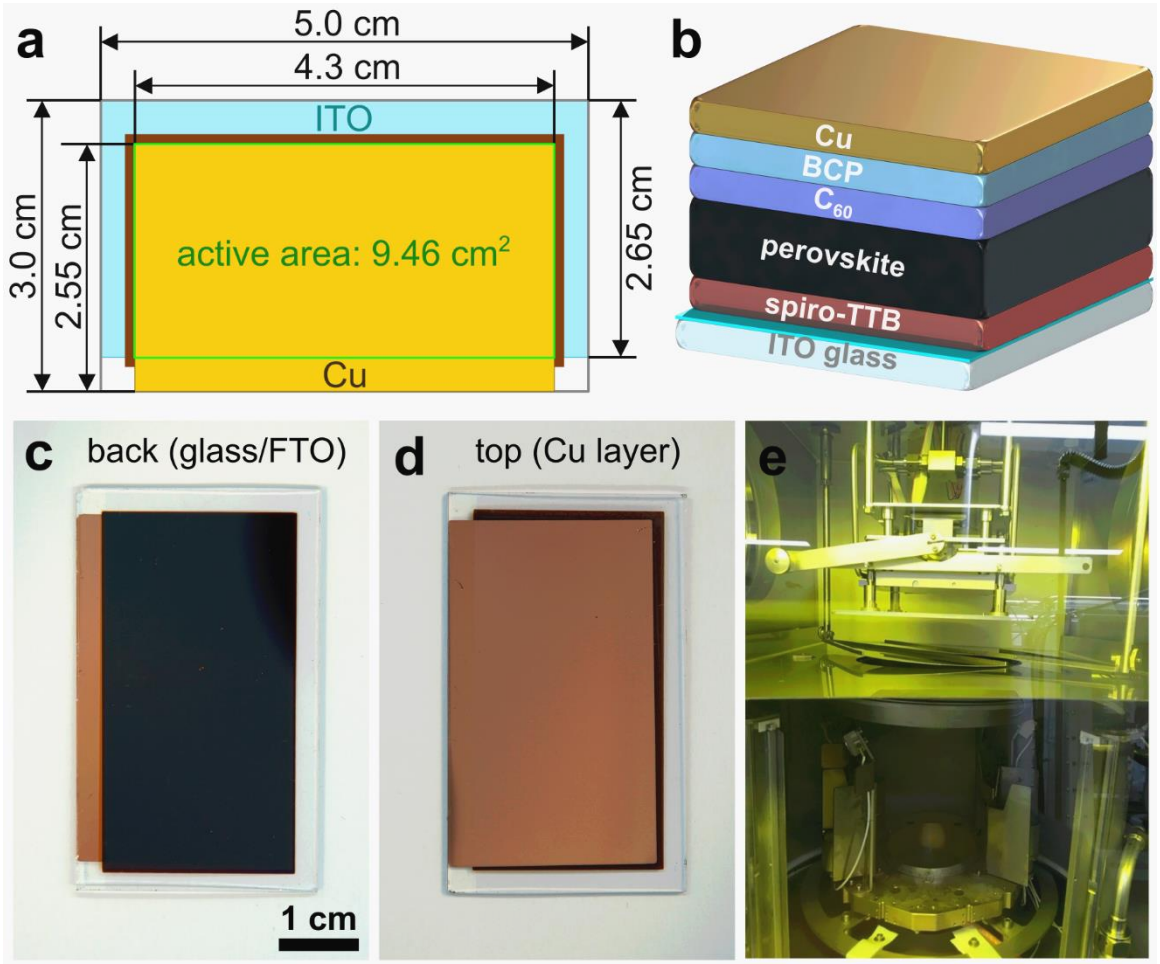

Figure S1. Perovskite PV device with a 9.46 cm^2 photoactive area. (a) Schematic showing the dimensions. (b) Illustration of the device structure. (c,d) Photographs of PV cells. (e) Perovskite evaporation chamber.

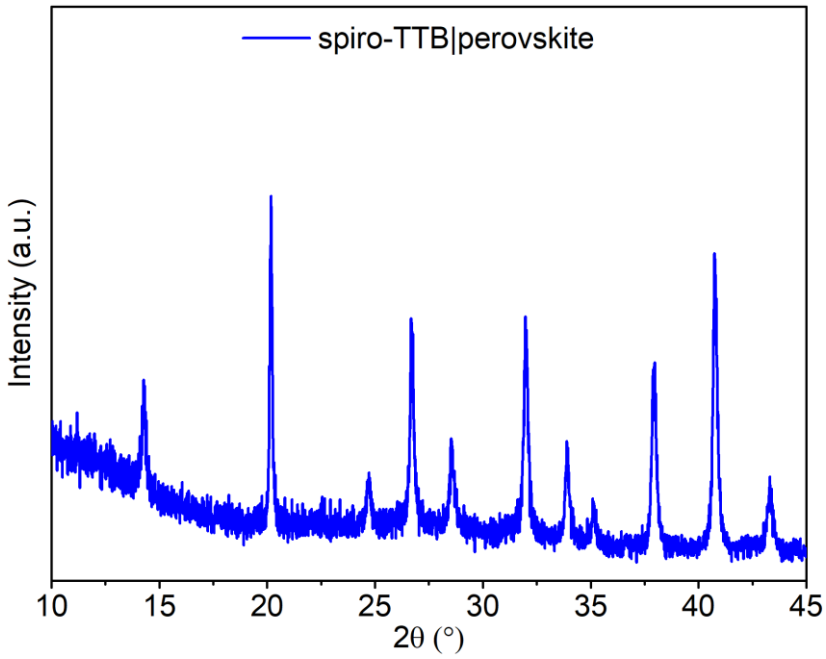

Figure S2. X-ray diffraction (XRD) analysis of the fully evaporated perovskite film. The $FA_{0.7}Cs_{0.3}Pb(I_{0.9}Br_{0.1})_3$ perovskite is deposited onto ITO|spiro-TTB, as encountered in a complete PV device.

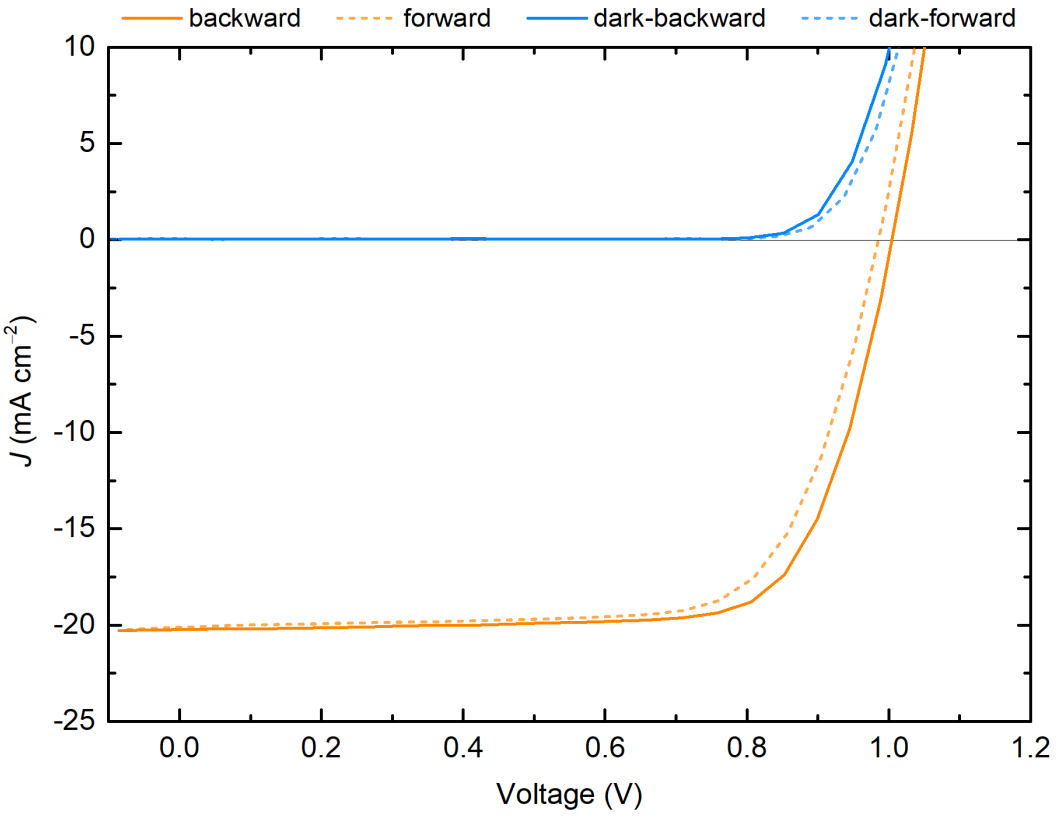

Figure S3. *JV* scans of a representative ITO|spiro-TTB|perovskite|C_{60}|BCP|Cu PV device with a 0.12 cm^2 active area. A small hysteresis is observed between forward and backward scans.

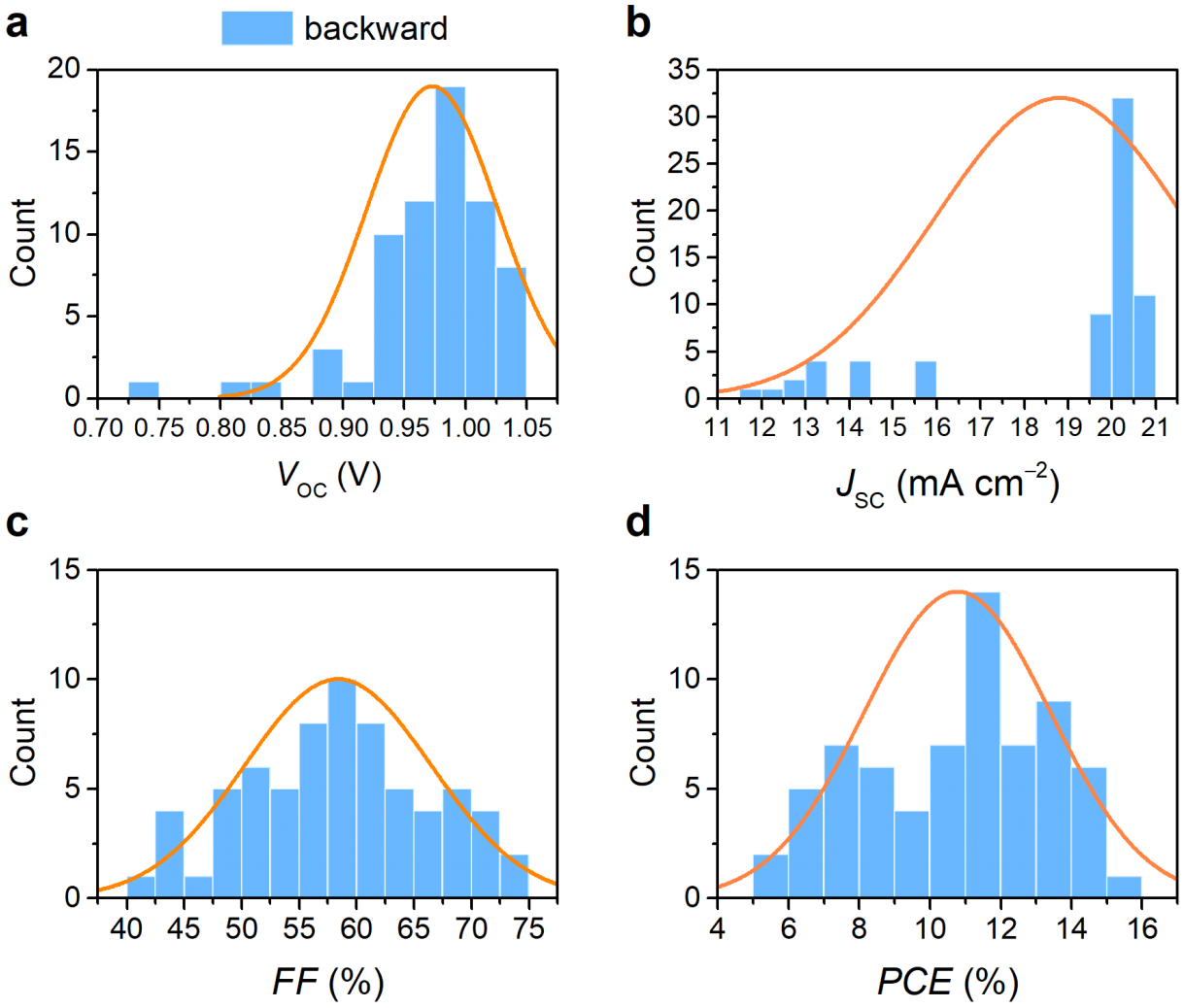

Figure S4. Histograms for the PV parameters of 68 small-scale evaporated perovskite cells. (a) Open-circuit voltage (V_{OC}). (b) Short circuit current density (J_{SC}). (c) Fill factor (FF). (d) Photovoltaic cell efficiency (PCE). Normal distribution curves are depicted in orange.

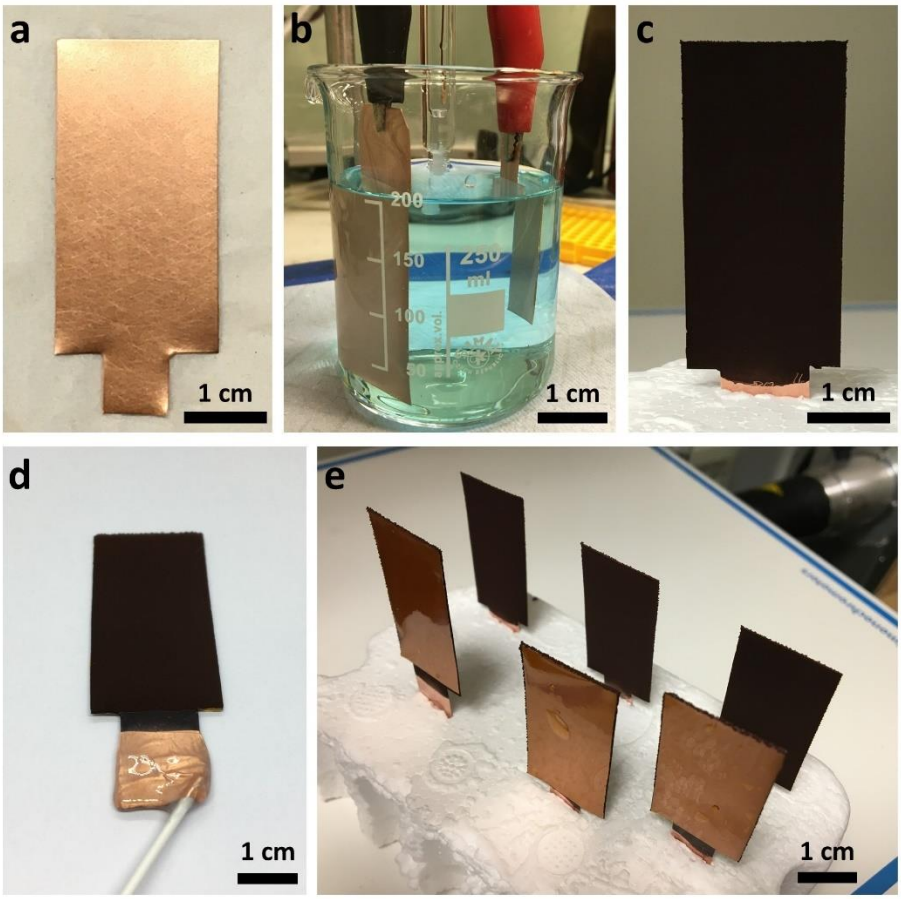

Figure S5. Catalyst preparation procedure. (a) An electropolished 10 cm^2 Cu foil substrate which was masked on one side by Kapton tape. (b) Deposition bath with a Ag/AgCl reference electrode, a 42 cm^2 Cu foil counter electrode, and a 10 cm^2 electropolished Cu foil substrate as working electrode dipped in precursor salt solution. (c) A 10 cm^2 CuIn alloy catalyst after electrodeposition. (d) CuIn electrode connected to a wire prior to the electrochemical test. (e) A batch of six 10 cm^2 $Cu_{92}In_8$ catalysts showing both the catalyst side as well as the Kapton masked back side of the Cu foil substrate.

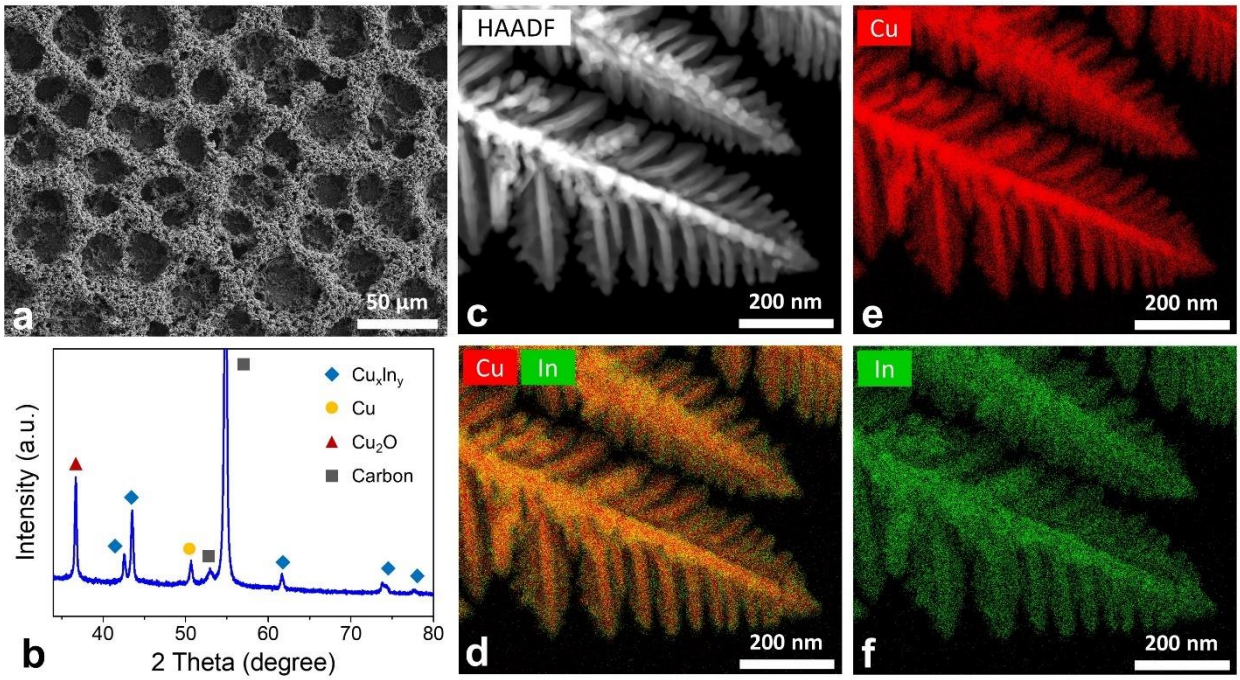

Figure S6. Physical characterisation of the 10 cm^2 $Cu_{92}In_8$ bimetallic alloy catalyst. (a) Scanning electron microscopy (SEM) image shows the overall microporous structure. (b) XRD analysis of the as-prepared CuIn alloy catalyst. (c) High-angle annular dark field (HAADF) image of dendrites. (d-f) Scanning transmission electron microscopy (STEM) mapping demonstrates a bimetallic (d), Cu (e), and In (f) distribution on dendrite surfaces.

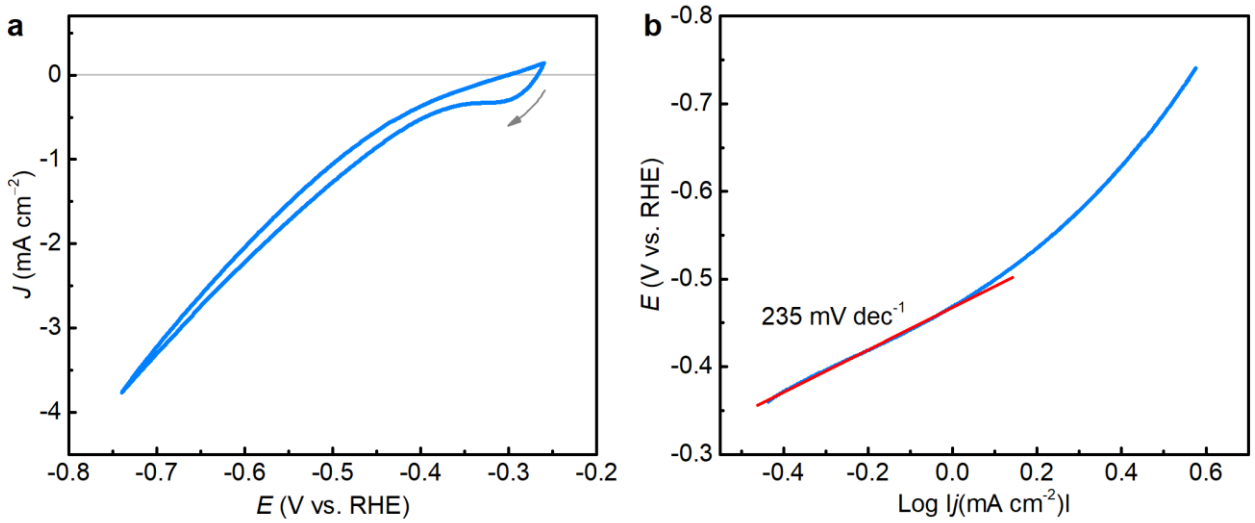

Figure S7. Post electrolysis cyclic voltammogram (CV) of the 10 cm^2 $Cu_{92}In_8$ catalyst. (a) The CV trace indicates a very low catalyst overpotential, with an onset at around −0.3 V vs. RHE. CV is recorded in CO_2 saturated 0.5 M $KHCO_3$, pH 7.4, at a 25 mV s^{-1} scan rate. Gray arrow indicates starting point and direction of the CV scan. (b) Corresponding Tafel plot showing the Tafel slope (red line) for the faradaic process at moderate overpotentials.

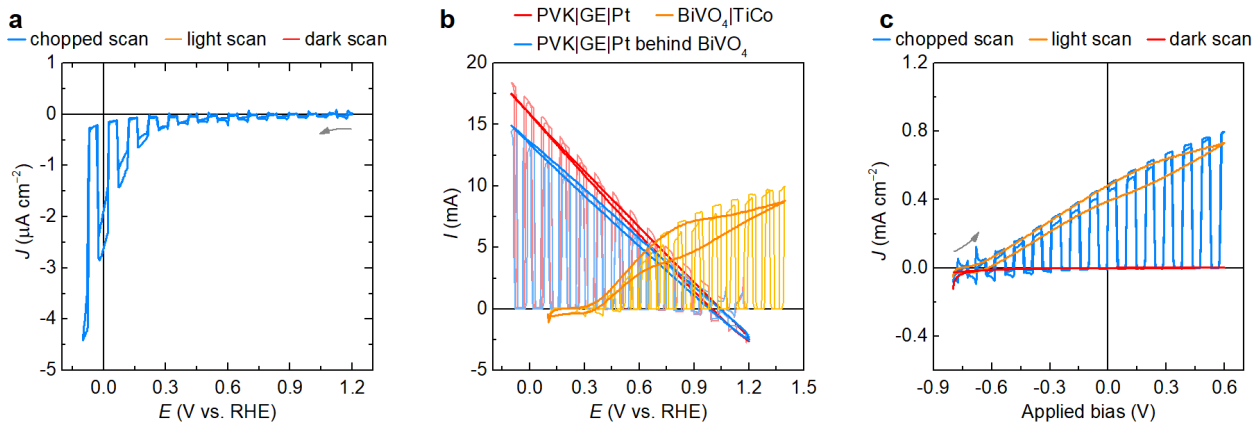

Figure S8. CV scans of a 10 cm^2 $BiVO_4$-PVK|GE|Pt tandem device and its corresponding photoelectrodes. (a) CV scan of a PVK|GE photocathode under chopped light irradiation. Negligible currents are observed in the absence of a catalyst. (b) CVs of PVK|GE|Pt and $BiVO_4$ photoelectrodes. The sign of photocathode traces is reversed to illustrate photocurrent overlap. Only a small change in current is observed when the photocathode is covered by $BiVO_4$, indicating that the overall photocurrent is limited by resistive losses rather than photon flux. (c) CVs of the resulting perovskite-$BiVO_4$ tandem device in a 2-electrode configuration. CVs are recorded under continuous or 5 s on - 5 s off chopped light irradiation (1 sun, AM 1.5G, 100 mW cm^{-2}) in a 0.1 M KB_i, 0.1 M K_2SO_4 solution, under N_2, pH 8.50, room temperature.

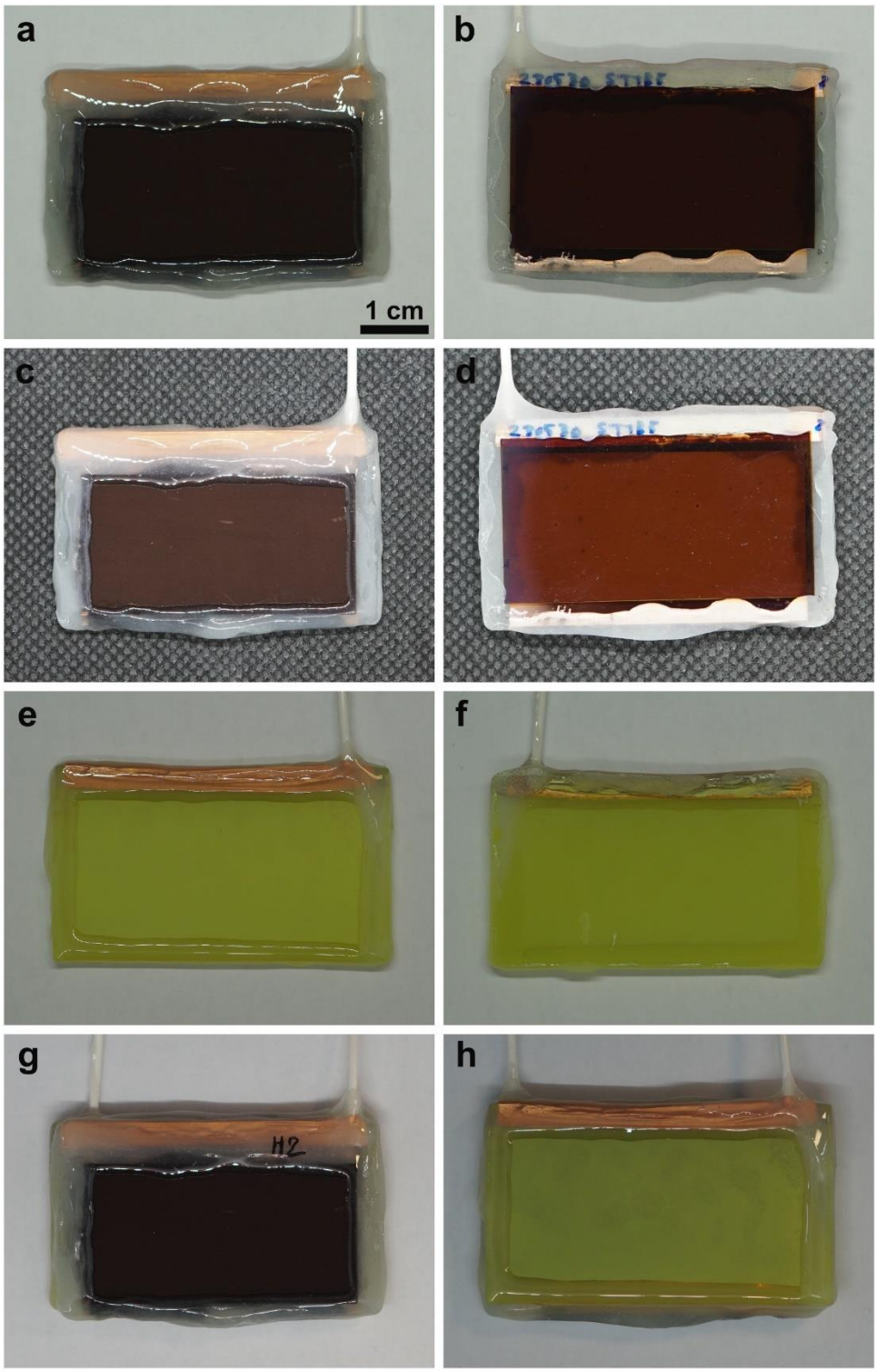

Figure S9. Photographs of the 10 cm^2 PEC systems. (a-d) Perovskite photocathodes: (a,c) - $Cu_{92}In_8$ alloy for CO_2 reduction, (b,d) - view from the glass side. (e,f) $BiVO_4$ photoanode for O_2 evolution. (g,h) Perovskite-$BiVO_4$ tandem device shown from: (g) - the CuIn catalyst, (h) - the $BiVO_4$ side.

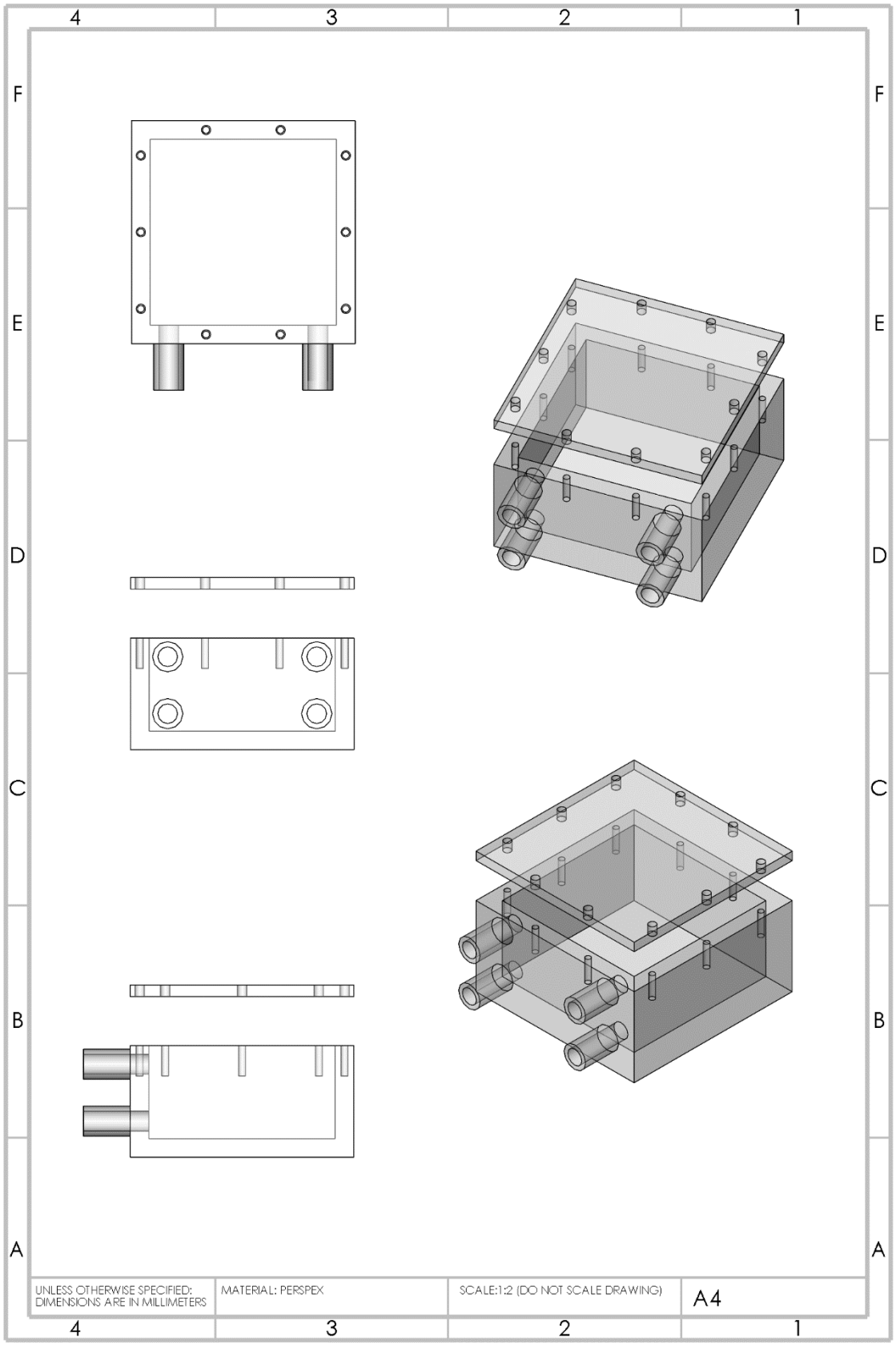

Figure S10. Schematic projections of the 9.6×9.6 cm^2 Perspex reactor. The reactor has an inner volume of 8×8×4 cm^3.

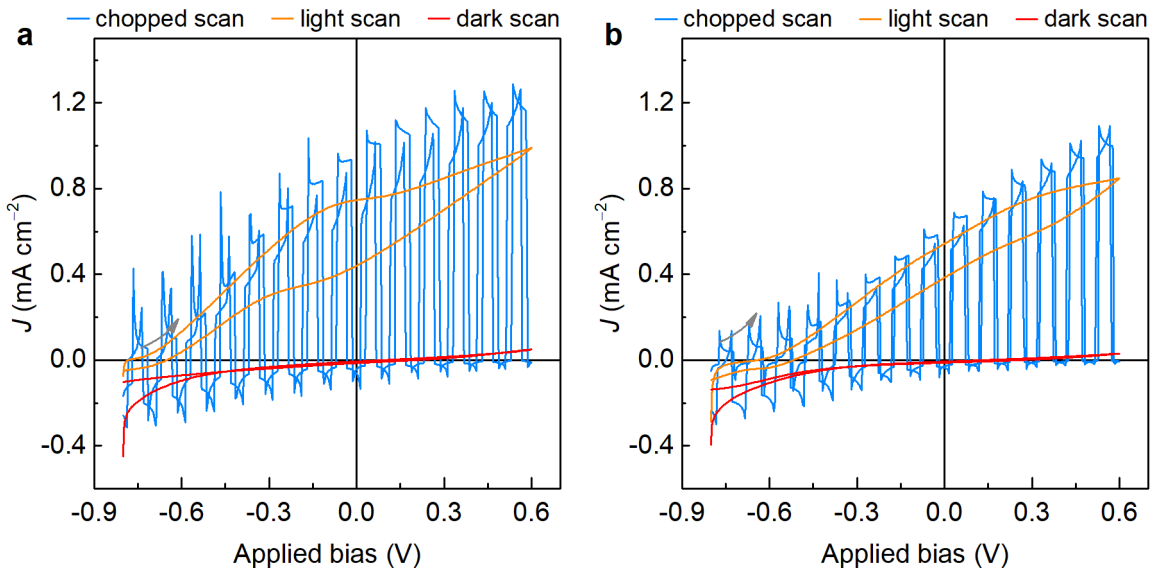

Figure S11. CV scans of a 10 cm^2 $BiVO_4$-PVK|GE|Pt PEC tandem device under chopped, continuous and no light irradiation. (a) Before chronoamperometry. (b) After 10 h CPE under 0 V applied bias voltage (1 sun, AM1.5G, 100 mW cm^{-2}; 0.1 M KB_i, 0.1 M K_2SO_4, under N_2, pH 8.50, room temperature).

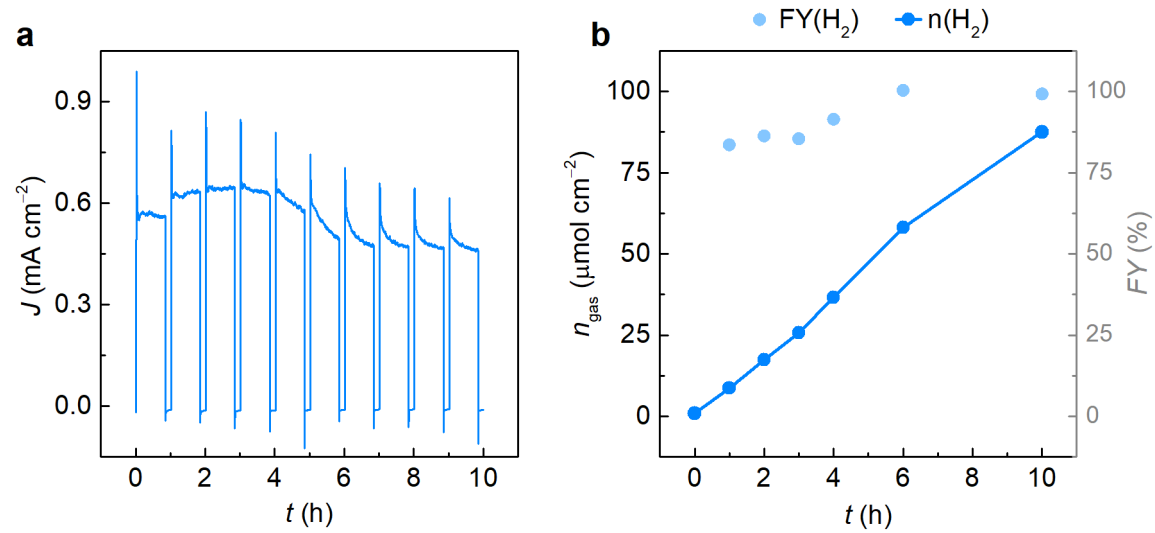

Figure S12. Unassisted water splitting with a 10 cm^2 $BiVO_4$-PVK|GE|Pt tandem device. (a) 10 h CPE at 0 V applied bias. (b) Time dependent amounts of H_2 and faradaic yield. CPE test is conducted under 50 min on - 10 min off chopped irradiation (1 sun, AM 1.5G, 100 mW cm^{-2}) in a 0.1 M KB_i, 0.1 M K_2SO_4 solution, under N_2, pH 8.50, room temperature.

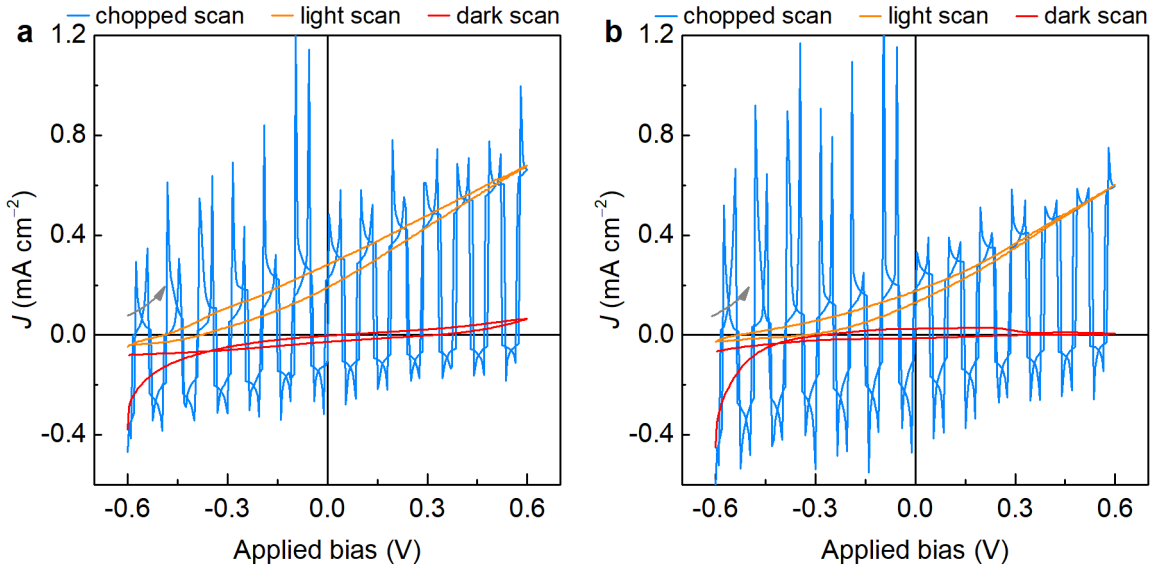

Figure S13. CVs of a 10 cm^2 $BiVO_4$-PVK|GE|$Cu_{92}In_8$ tandem device. (a) Before chronoamperometry. (b) After a 36 h long-term CPE test at 0 V applied bias voltage. Traces are recorded under continuous, chopped and no light irradiation (1 sun, AM 1.5G, 100 mW cm^{-2}), in 0.5 M $KHCO_3$, under CO_2, pH 7.4, at room temperature.

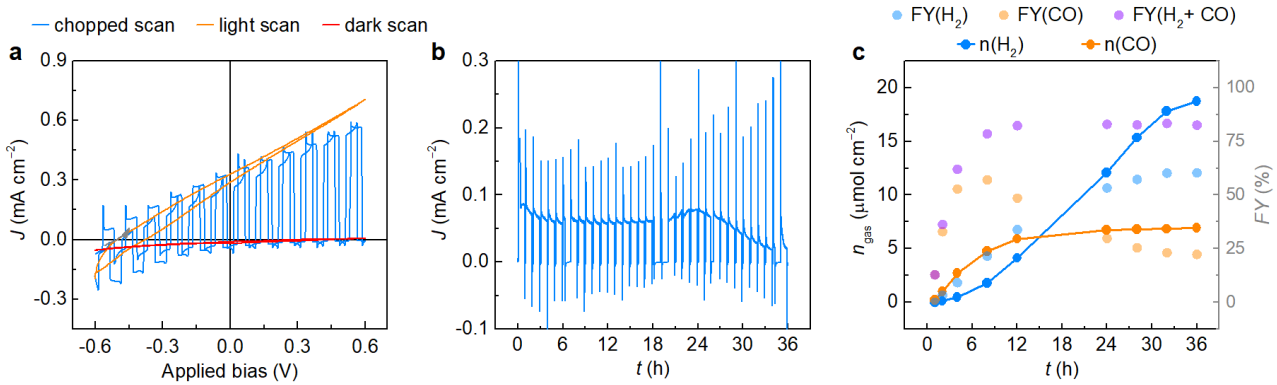

Figure S14. Photoelectrochemical tests of 10 cm^2 $BiVO_4$-PVK|GE|$Cu_{92}In_8$ tandem devices. (a) CVs of a 10 cm^2 $BiVO_4$-PVK|GE|$Cu_{92}In_8$ tandem device. (b,c) Long-term CPE test of a second $BiVO_4$-PVK|GE|$Cu_{92}In_8$ tandem device (b), with corresponding FYs and product amounts (**c**). Traces are recorded under 1 sun irradiation (AM 1.5G, 100 mW cm^{-2}), in 0.5 M $KHCO_3$, under CO_2, pH 7.4, at room temperature.

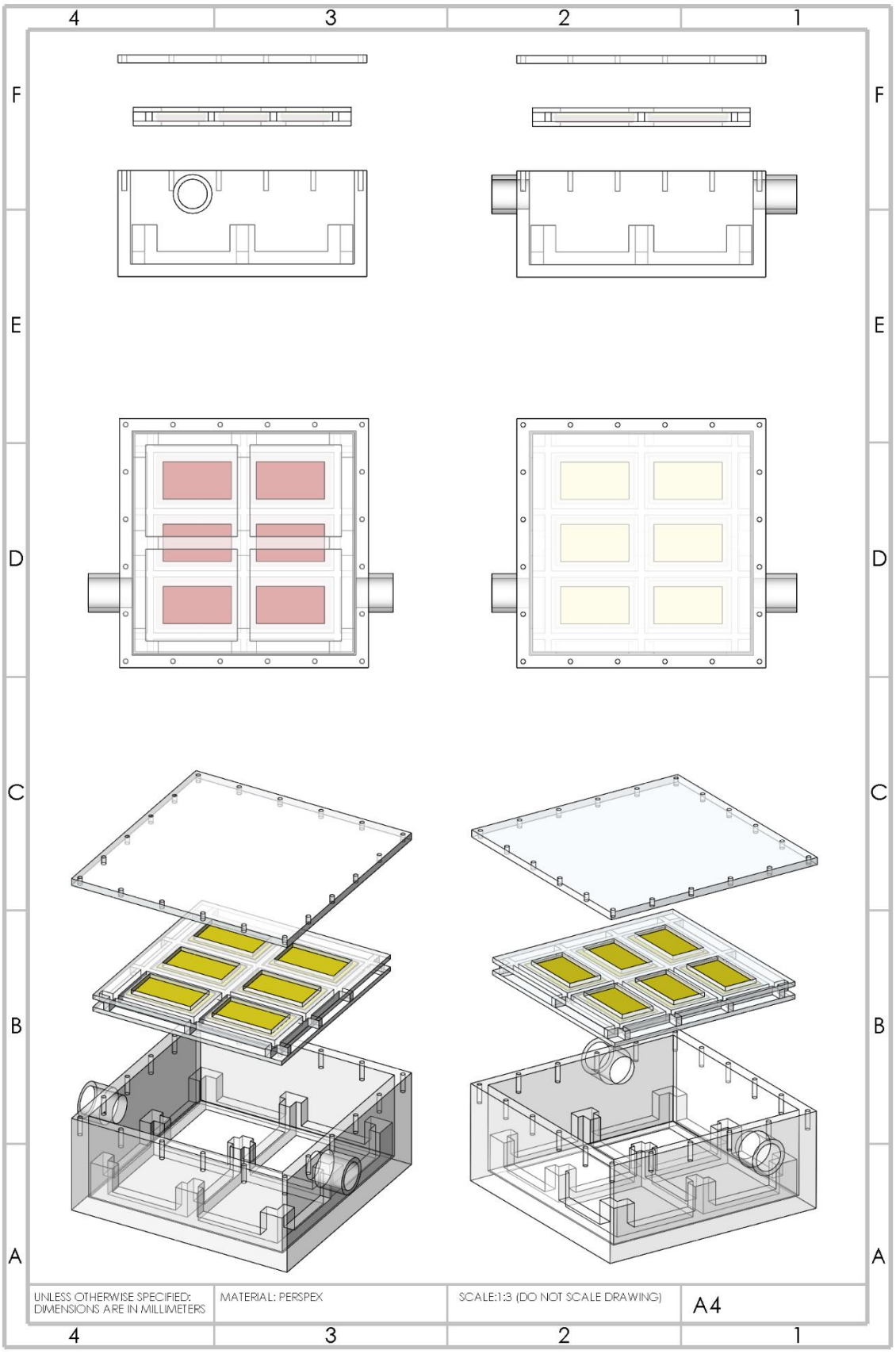

Figure S15. Schematic projections of the 16×16 cm^2 Perspex reactor. The reactor has an inner volume of 14.4×14.4×6 cm^3.[1]

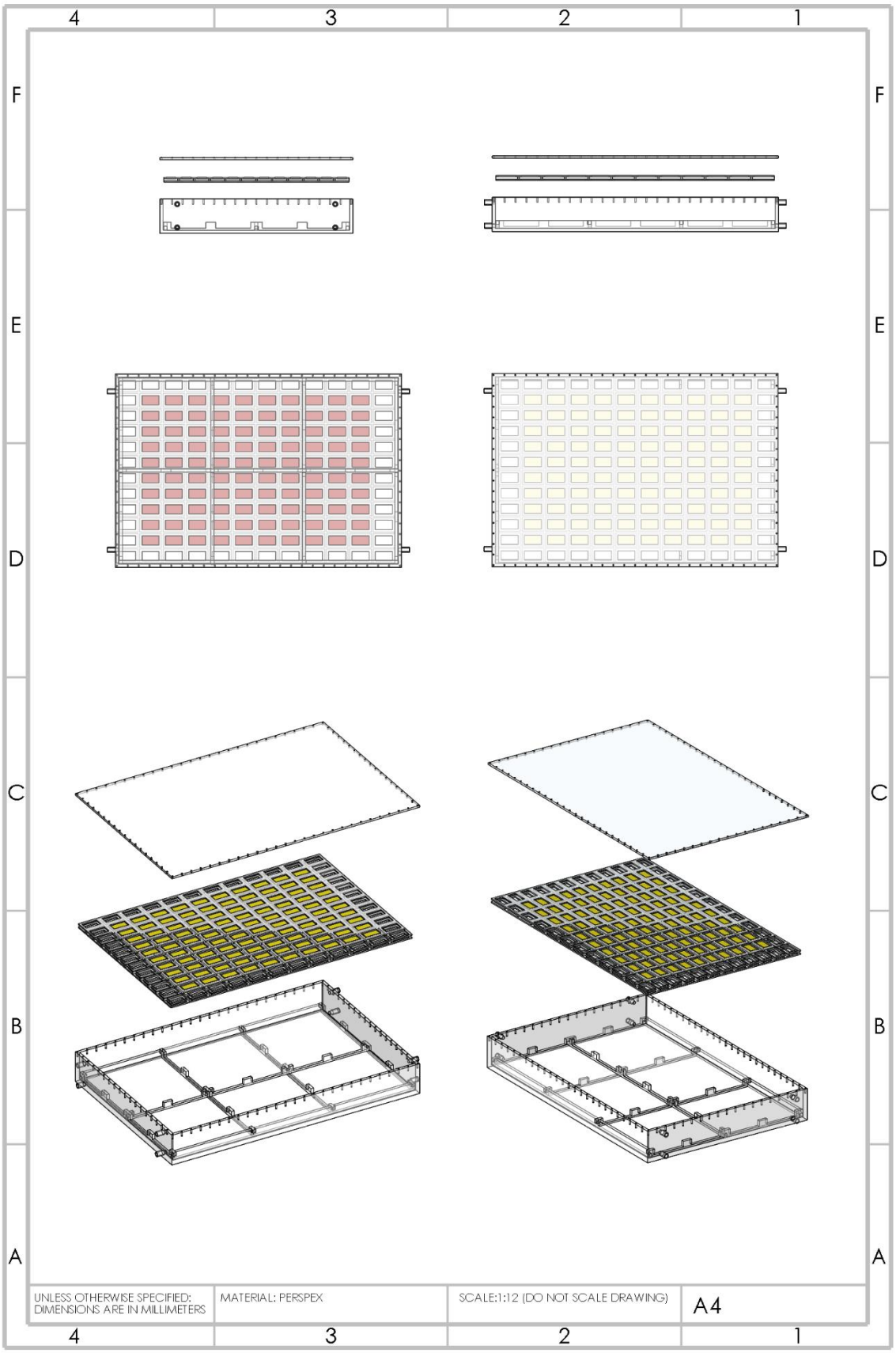

Figure S16. Schematic projections of the 0.7×0.5 m^2 Perspex reactor.

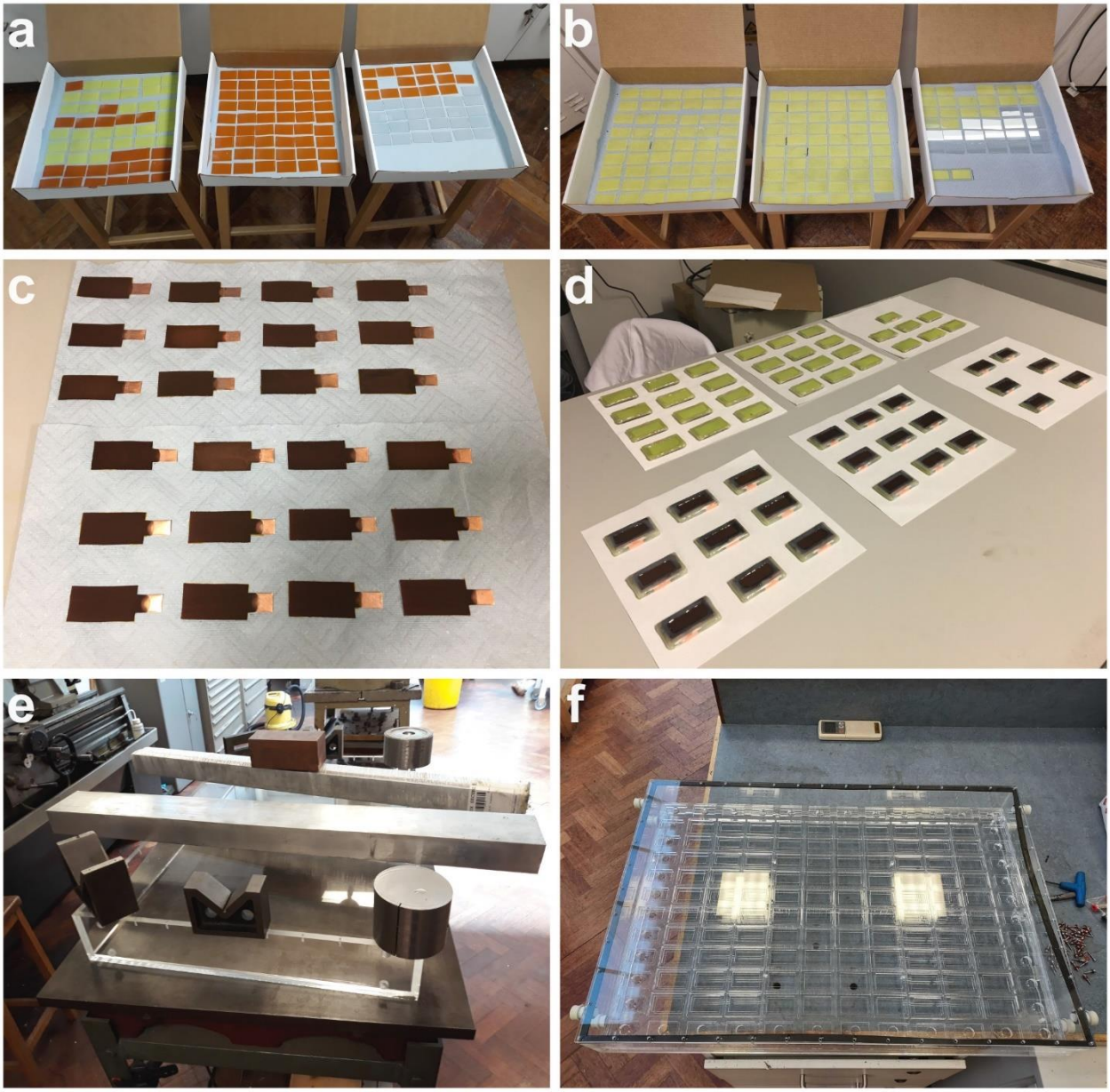

Figure S17. Stepwise sample and reactor preparation for the final outdoor demonstration of the EIC Horizon Prize. (a,b) Deposition of >100 $BiVO_4$ photoanodes on 5×3 cm^2 FTO glass substrates. BiOI was deposited over the FTO glass over the course of 3 days. The electrodes were next annealed in the presence of a vanadium source, in batches of 16, to form the $BiVO_4$ electrodes (see Methods). (a) Two $BiVO_4$ batches are completed. (b) All electrodes are ready. (c) Two batches of 10 cm^2 electrodeposited CuIn alloy catalysts. (d) Assembled 'artificial leaf' devices. (e,f) Construction of the 0.7×0.5 m^2 reactor from Perspex panels at the Mechanical Workshop of the Yusuf Hamied Department of Chemistry, University of Cambridge.

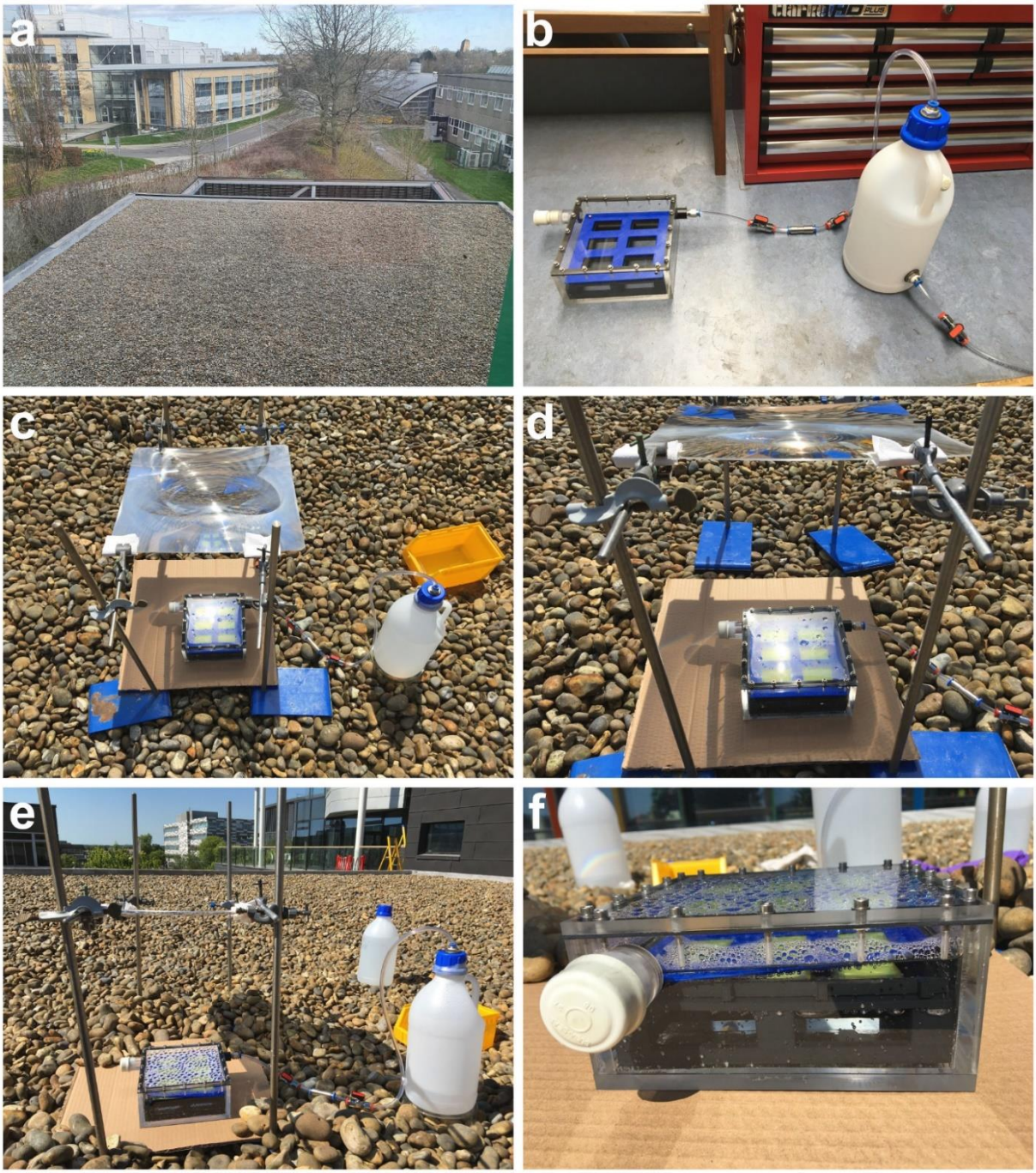

Figure S18. Medium-scale outdoor test with a 3×2 array reactor on the roof of the Maxwell Centre, University of Cambridge. (a) Overview of the testing area. (b) Experimental setup. The reactor is connected to a 2.5 L gas collection tank. The tank is initially filled with 1 M KOH solution, which is meant to absorb CO_2 from the gas mixture, so only pure syngas is collected in the tank's headspace. An outlet for displaced KOH solution is found close to the bottom of the tank. In this arrangement, the outlet tube must be placed above the liquid level in the tank, to only allow KOH release in case of gas overpressure, following Pascal's principle. (c-e) Experimental setup under operation, with a 39.5×39.5 cm^2 Fresnel lens for light concentration. In the absence of a solar tracking system, the focal point drifts away from the reactor area over a couple of hours (e). This can prevent light concentration or even induce a shadowing effect, hence, the Fresnel lens is removed for the remainder of the test. (f) Close-up photograph showing syngas bubble accumulation underneath the artificial leaves, and optical loses due to condensed water droplets on the window of the reactor.

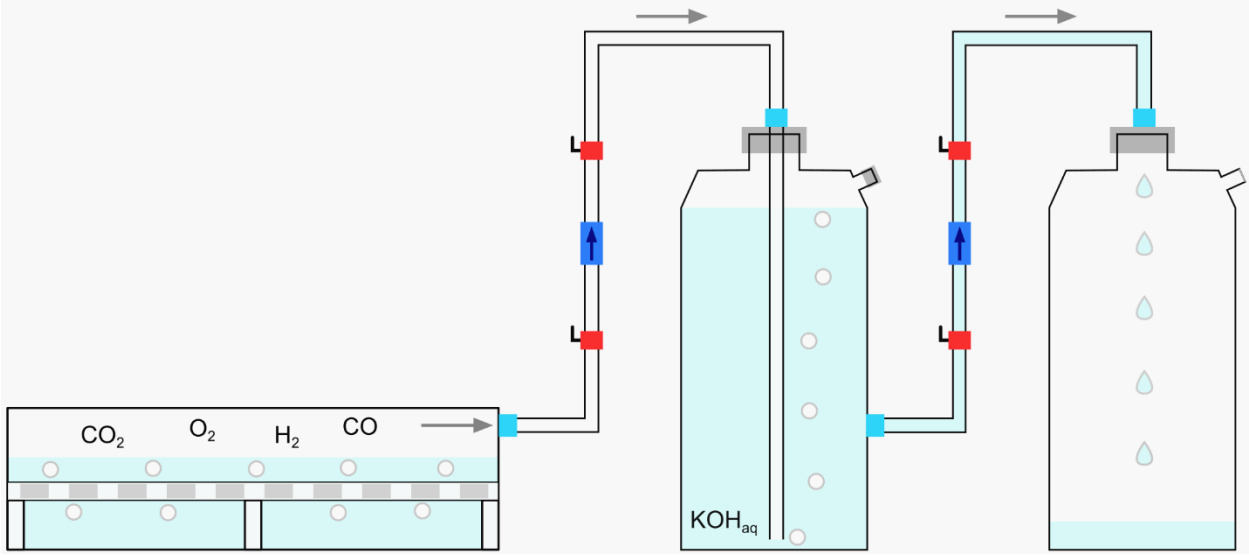

Figure S19. Schematic of the overall PEC system for product collection and CO_2 removal. The PEC reactor is connected to a KOH tank which removes CO_2 from the reaction mixture, and a second tank for collection of displaced KOH. On-off (red) and one-way valves (blue) were mounted along the tubing to ensure the one-directional flow of fluids. The push fit valves and fittings (light blue) are used to connect the rubber tubing to the reactors and gas tanks. However, these connectors have been found to be leaky to both liquids and gases during outdoor tests.

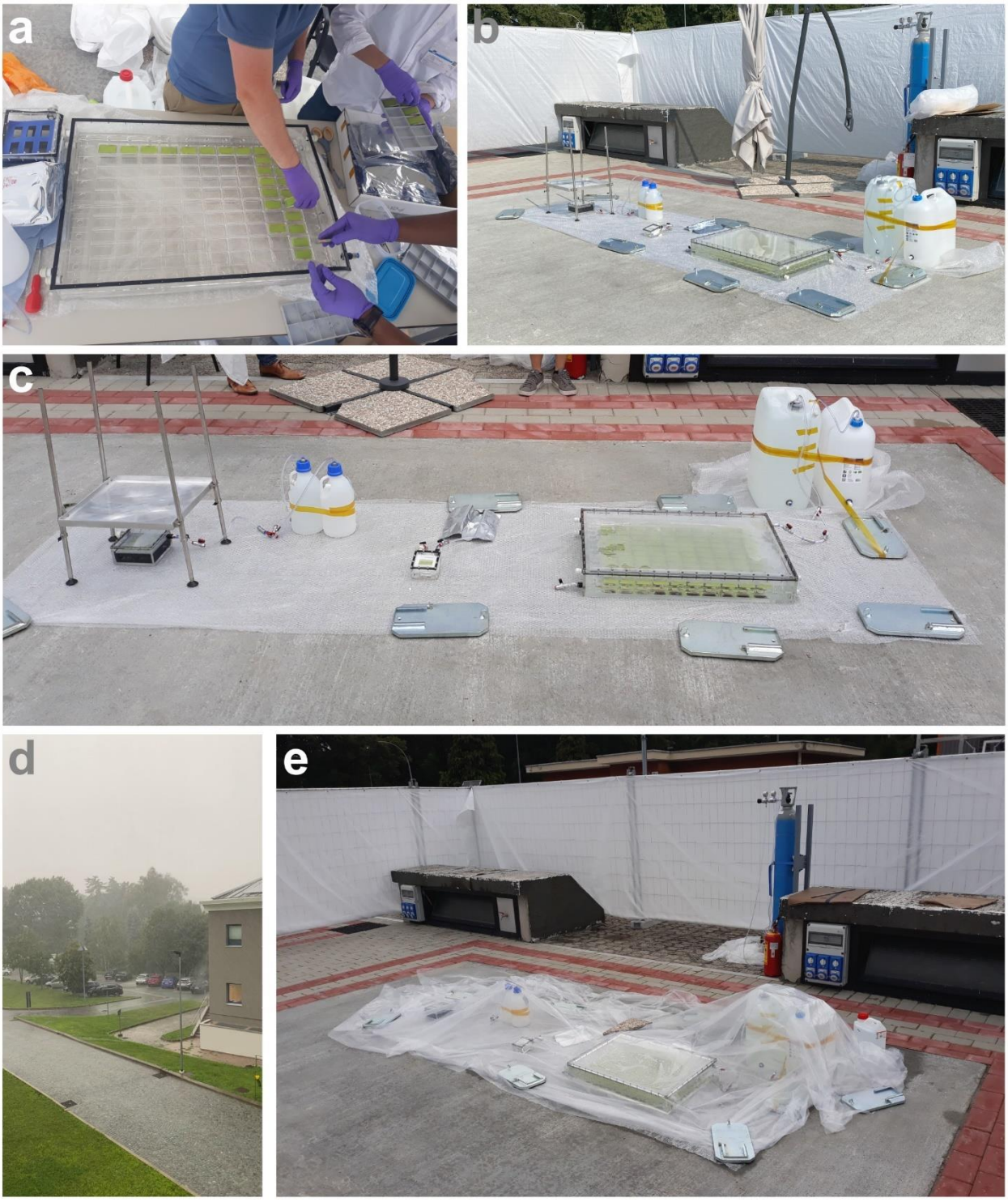

Figure S20. Photographs of the experimental setup during the outdoor test in Ispra, Italy. (a) Loading the 100 'artificial leaf' samples into the 0.7×0.5 m^2 reactor. (b,c) Complete setup at the beginning of the 3-day test. Left: medium-scale, 3×2 array reactor with a 39.5×39.5 cm^2 Fresnel lens for light concentration, and 2.5 L gas and KOH collection tanks. Centre: 9.6×9.6 cm^2 reactor with a single artificial leaf device. The reactor is connected to a gas sampling bag for product collection. Right: large-scale, 0.35 m^2 reactor. The large reactor is connected to a 25 L gas tank, initially filled with 1 M KOH, and a 20 L empty tank for collecting the displaced KOH solution. All tubing is secured by one-way valves and manual on-off valves. (d) Storm during the first day of testing. (e) The setup is covered with plastic foil to prevent damage from the strong rain and wind.

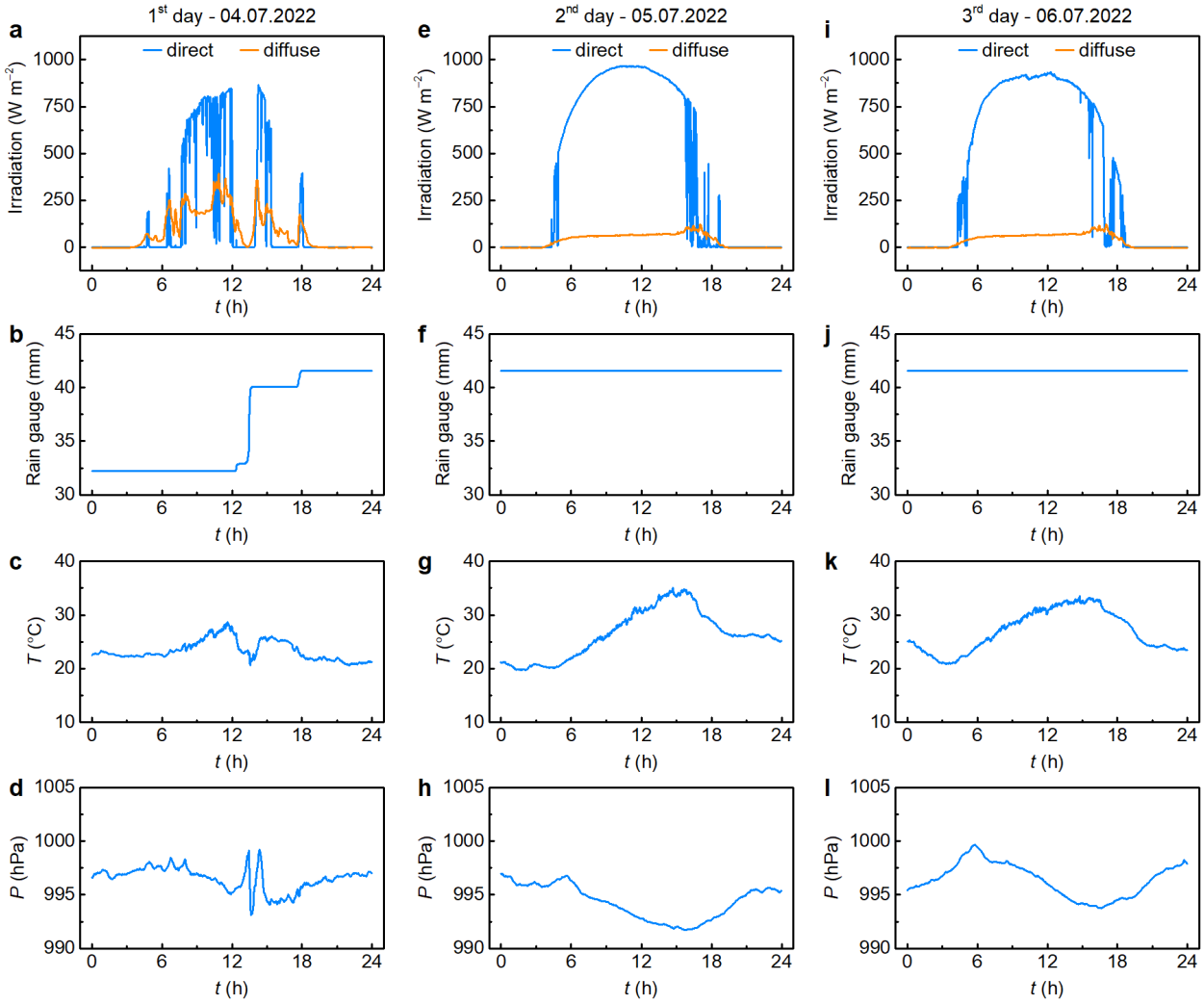

Figure S21. Weather conditions during the 3-day outdoor test in Ispra, Italy. Data is recorded on: (a-d) the 1st day; (e-h) 2nd day; (i-l) 3rd day. (a,e,i) Direct and diffuse irradiation. (b,f,j) Rain gauge, indicating the extent of the first-day storm. (c,g,k) Ambient temperature. (d,h,l) Local barometric pressure. ESTI Meteo Tower Data is provided by Diego Pavanello (Joint Research Centre, European Solar Test Installation, Ispra, Italy), and can be accessed under: https://re.jrc.ec.europa.eu/meteo/meteo.php.

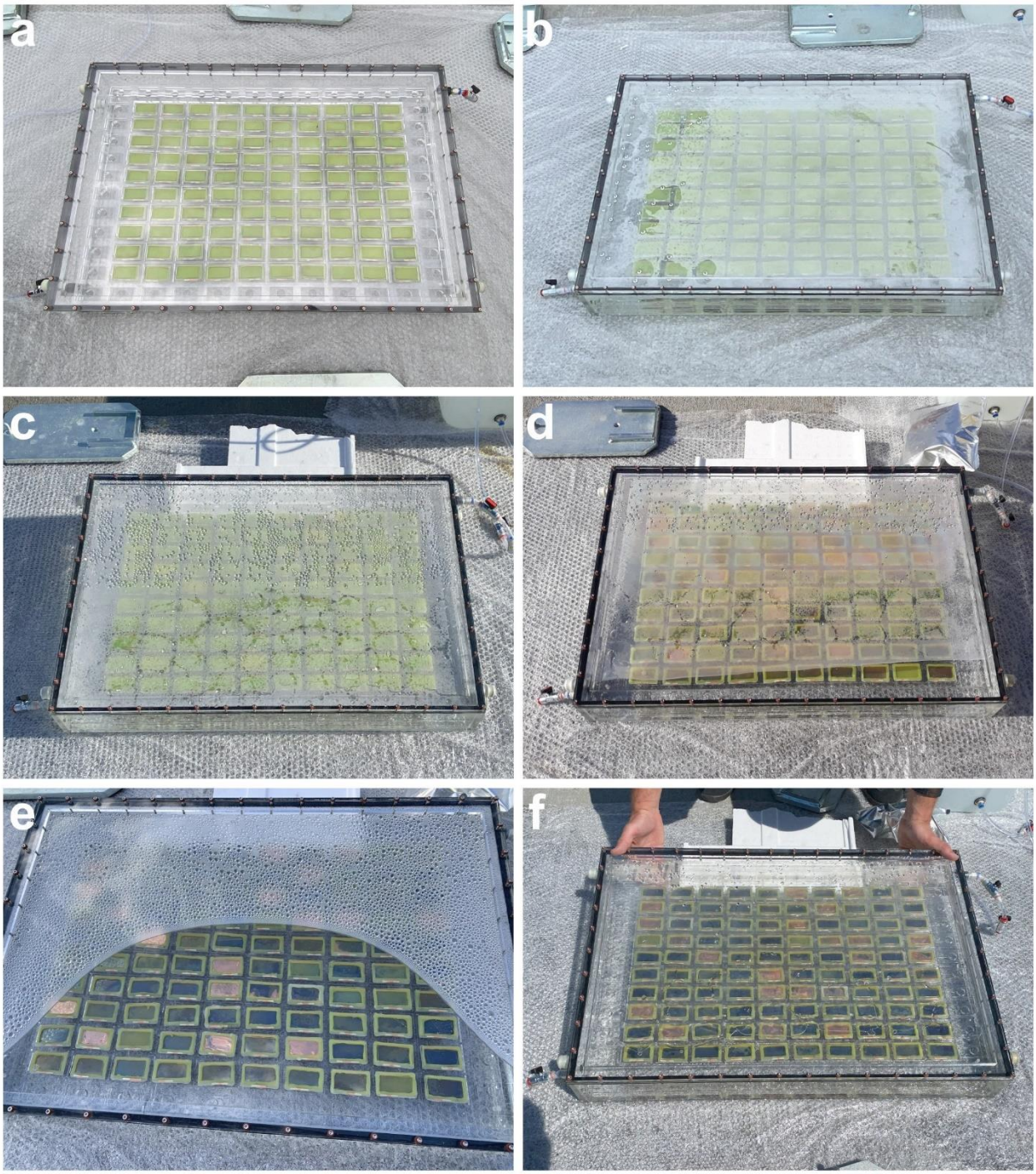

Figure S22. Photographs of the 10×10 'artificial leaf' array reactor during the outdoor test in Ispra, Italy. (a) Pristine reactor without electrolyte solution. (b) Reactor filled with 0.5 M $KHCO_3$ buffer solution, at the beginning of the three-day test (09:05, 4th July 2022). (c) Reactor valve is open to the collection tank at the start of the second day (08:51, 5th July 2022). (d) $BiVO_4$ corrosion after KOH leakage into the reactor from the collection tank (17:29, 5th July 2022). Leakage started in the morning, due to slight underpressure from the overnight temperature decrease. (e) The basic solution pulls CO_2 from the head space, creating underpressure, which bends the acrylic glass lid and pulls further KOH solution into the reactor. (f) $BiVO_4$ degradation under the basic solution reveals perovskite sample degradation (11:39, 6th July 2022). The metallic copper samples reveal complete perovskite dissolution, whereas the dark samples preserved the perovskite layer.

Table S1. Comparison between the performance of reported photo(electro)catalytic artificial leaves for water splitting and CO_2 reduction to C_1 products. [a] Separate long-term tests. Abbreviations: ePVK – evaporated perovskite device; fPVK – flexible perovskite device; H_2ase – hydrogenase; CoMTPP, CotpyP – cobalt-based molecular catalysts; CNT – carbon nanotubes.

Sample	J ($mA\ cm^{-2}$)	STF (%)	n ($\mu mol\ cm^{-2}$)	Stability (h)	Area (cm^2)	Product	Comments	Ref.
$BiVO_4$ – ePVK|GE|$Cu_{92}In_8$	0.13	0.032	9.36	36	10	CO	syngas + water	this
		0.098	39.4			H_2	splitting	work
$BiVO_4$ – ePVK|GE|Pt	0.56	0.69	87.5	10	10	H_2	water splitting	this work
$BiVO_4$ – BiOI|GE|$Cu_{92}In_8$	0.094	0.045	6.5	12 (72[a])	0.225	CO	syngas + water	2
		0.042	6.6			H_2	splitting	
Ti|$BiVO_4$ –	0.07	0.053	4.48	10 (24[a])	1.7	CO	syngas + water	1
fPVK|GE|CoMTPP@CNT		0.021	1.94			H_2	splitting	
		0.053	2.24			O_2		
Ti|$BiVO_4$ – fPVK|GE|Pt	0.58	0.578	60.4	10	1.7	H_2	water splitting	1
		0.401	19.9			O_2		
$BiVO_4$ – PVK|GE|$Cu_{96}In_4$	0.195	0.19	21.17	10	0.25	CO	syngas + water	3
		~0.06	7.21			H_2	splitting	
		–	14.71			O_2		
$BiVO_4$ – PVK|FM|CoMTPP@CNT	0.18	0.018	1.8	10 (67[a])	0.25	CO	syngas + water	4
		0.056	5.8			H_2	splitting	
		0.146	6.8			O_2		
$BiVO_4$ – PVK|FM|H_2ase	1.1	1.1	21.2	10	0.25	H_2	water splitting	5
		0.677	9			O_2		
$BiVO_4$ – PVK|FM|Pt	0.39	0.35	–	18	0.25	H_2	water splitting	6
$BiVO_4$ – PVK|FM|Pt	0.23	0.15	–	1 - 14	10	H_2	water splitting	6
Cr_2O_3/Ru-$SrTiO_3$:La,Rh/Au/$BiVO_4$:		1.1	196	10	7.5	H_2	water splitting	7
Mo sheets		–	98			O_2		
CotpyP/$SrTiO_3$:La,Rh/Au/$BiVO_4$:		0.08	6.53	6	1	HCOOH	aqueous formate	8
Mo/RuO_2 sheets		–	0.18			H_2	production	
		–	3.12			O_2		

Movie S1. Gas evolution during laboratory tests of perovskite-$BiVO_4$ tandem devices for water splitting and CO_2 reduction.

Movie S2. Overpressure from the medium-scale reactor is released as gas bubbles in a 2.5 L gas tank. The test was performed on the roof of the Maxwell Centre, University of Cambridge.

Discussion S1. Guidelines of the EIC Horizon Prize "Fuel from the Sun: Artificial Photosynthesis".

According to the Rules of Contest (released on 6 December 2017) and EIC infographic, the focus of the Horizon Prize was awarding the best technology that produced sustainable fuel by combining sunlight, water and carbon dioxide. Fully functional proof-of-concept prototypes needed to integrate the whole artificial photosynthesis process from light capture to fuel production. Accordingly, while no target was set for the carbon content in the product mixture, established PV-electrolysers and water splitting systems were not eligible for the competition.

The prize was awarded based on five evaluation criteria.
a) Degree of system integration from light capture to fuel production (integrity, durability and novelty).
b) Device/system performance (efficacy, efficiency).
c) Production of fuel that will be used in an engine (autonomous operation in respect of energy use).
d) Widest market potential (evaluated by applicants based on a life-cycle assessment):

- materials consumed, in particular toxic, hazardous or rare earth elements;
- water consumption;
- emissions to air;
- waste production, including hazardous waste.

e) Commercial potential of the device:

- replicability outside the competition conditions to support wide market applicability;
- upscaling and roll-out potential within a tangible timeframe;
- prospects of commercial viability in the near future;
- cost analysis and prospects at commercial scale.

The shortlisted teams were next evaluated during the competition Grand Final based on the following.
a) Participants would transport each device to JRC Ispra and set it up on an outdoor pad not exceeding 5×5 m^2 and 3 m in height. A maximum of 48 h was allowed for set-up and commissioning/initial testing.
b) Inspection of the device by expert jurors to verify its design, materials use and inputs during set-up and commissioning.
c) Simultaneous unassisted operation of all devices for a continuous period of 72 h using natural sunlight. Pure CO_2 at a pressure of 1 atm, mains electricity and water was supplied to all test pads.
d) Evaluation of the fuel produced over 72 h through its combustion and powering a Stirling engine.

Supplementary References

1 V. Andrei, G. M. Ucoski, C. Pornrungroj, C. Uswachoke, Q. Wang, D. S. Achilleos, H. Kasap, K. P. Sokol, R. A. Jagt, H. Lu, T. Lawson, A. Wagner, S. D. Pike, D. S. Wright, R. L. Z. Hoye, J. L. MacManus-Driscoll, H. J. Joyce, R. H. Friend and E. Reisner, *Nature*, 2022, **608**, 518–522, https://doi.org/10.1038/s41586-022-04978-6.

2 V. Andrei, R. A. Jagt, M. Rahaman, L. Lari, V. K. Lazarov, J. L. MacManus-Driscoll, R. L. Z. Hoye and E. Reisner, *Nat. Mater.*, 2022, **21**, 864–868, https://doi.org/10.1038/s41563-022-01262-w.

3 M. Rahaman, V. Andrei, C. Pornrungroj, D. Wright, J. J. Baumberg and E. Reisner, *Energy Environ. Sci.*, 2020, **13**, 3536–3543, http://dx.doi.org/10.1039/D0EE01279C.

4 V. Andrei, B. Reuillard and E. Reisner, *Nat. Mater.*, 2020, **19**, 189–194, https://doi.org/10.1038/s41563-019-0501-6.

5 E. Edwardes Moore, V. Andrei, S. Zacarias, I. A. C. Pereira and E. Reisner, *ACS Energy Lett.*, 2020, **5**, 232–237.

6 V. Andrei, R. L. Z. Hoye, M. Crespo-Quesada, M. Bajada, S. Ahmad, M. de Volder, R. Friend and E. Reisner, *Adv. Energy Mater.*, 2018, **8**, 1801403.

7 Q. Wang, T. Hisatomi, Q. Jia, H. Tokudome, M. Zhong, C. Wang, Z. Pan, T. Takata, M. Nakabayashi, N. Shibata, Y. Li, I. D. Sharp, A. Kudo, T. Yamada and K. Domen, *Nat. Mater.*, 2016, **15**, 611, https://doi.org/10.1038/nmat4589.

8 Q. Wang, J. Warnan, S. Rodríguez-Jiménez, J. J. Leung, S. Kalathil, V. Andrei, K. Domen and E. Reisner, *Nat. Energy*, 2020, **5**, 703–710, https://doi.org/10.1038/s41560-020-0678-6.